Proceedings of IMECE2008
2008 ASME International Mechanical Engineering Congress and Exposition
October 31-November 6, 2008, Boston, Massachusetts, USA

IMECE2008-66292

EXPERIMENTAL ANALYSIS OF VIBRATION OF MICROMACHINED RESONATORS

Pezhman A. Hassanpour*
Department of Mechanical and Industrial Engineering, University of Toronto, 5 King's College Rd., Toronto, ON, Canada
Email: hassanpr@mie.utoronto.ca

Ebrahim Esmailzadeh
Faculty of Engineering and Applied Science, University of Ontario Institute of Technology, 2000 Simcoe Street North, Oshawa, ON, Canada

William L. Cleghorn
Department of Mechanical and Industrial Engineering, University of Toronto, 5 King's College Rd., Toronto, ON, Canada

James K. Mills
Department of Mechanical and Industrial Engineering, University of Toronto, 5 King's College Rd., Toronto, ON, Canada

ABSTRACT

Among many different mechanisms that are used for excitation and detection of vibration of micro-beam resonators, electrostatic comb-drives have the benefit of simplicity and large range of linear operation. The disadvantage of using comb-drives is the effect of added mass to the beam; however, the analytical model of the beam-mass system predicts that this shortcoming can be overcome by proper adjustment of the mass, rotary inertia, and location of the comb-drive. In addition, the analytical model can predict the effect of the axial force of the beam on the resonance frequencies. In this paper, the results of the experiments on two resonators are presented. These results are used to verify the validity of the analytical model and finding its parameters. Very close agreement between the theory and experiment is observed. The residual stress of the MEMS structural layer is measured using the calibrated analytical model parameters.

INTRODUCTION

Micromachined beams are widely used as resonant structures. A resonant structure, or resonator, is a structure designed to vibrate at a specified frequency usually one of its own natural frequencies. The natural frequencies of a resonator are its key design parameters, which in turn, are functions of the inertia and stiffness of the structure. The mass and modulus of elasticity of a solid structure are stable and highly robust properties; however, an applied force may change the stiffness. Consequently, this force can change the natural frequencies of the resonator.

Wide varieties of mechanisms and techniques are utilized to excite micro-beams and detect their vibrations, each of which has its own merits [1]. A commonly used excitation/detection mechanism is electrostatic actuation, where the electrostatic force can be applied to the beam by either directly applying an electric field to the beam resonator or attaching an electrostatic comb-drive actuator to the beam. A single-degree-of-freedom spring-mass model is considered to determine the fundamental natural frequency of a resonator excited by a comb-drive actuator. In addition, the finite element method was extensively used for the analysis of resonators although, little attention was paid to the higher modes of vibration, and the effect of the location of attached comb-drive with its dimension on the oscillatory behavior of the resonator. Recent investigations into the analytical model of the resonator have shown potential application for resonators working in their higher modes [2 and 3]. Modeling of the resonator as a continuous system has revealed that the mass, rotary inertia and the location of the comb-drive actuator have significant effects on the natural frequencies and the modes of vibration. In this study, the experimental results for the vibration of a set of micromachined resonators, fabricated by Micragem

* Corresponding author

Technology, are presented. The experimental results are compared with those obtained from the analytical model and a very close agreement between the theory and experiment is observed. The calibration of the theoretical model parameters by experimental results is discussed in detail. The calibrated model is used to measure the residual stress of the structural layer of the chip.

MECHANICAL MODEL

Fig. 1 shows an optical image of a resonant beam with attached comb-drive actuator/sensor at its mid-point. The MEMS electrical nodes are wire-bonded and the chip is glued to its package.

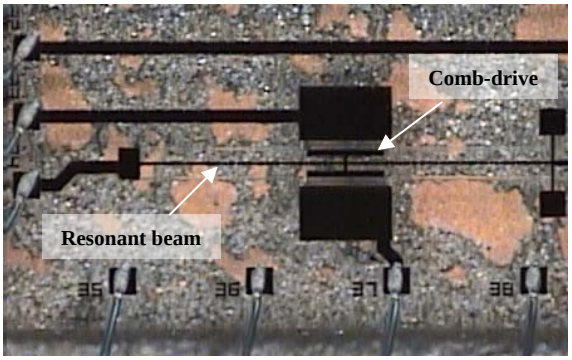

Fig. 1. A resonant beam with attached comb-drive actuator/sensor (ref. Table 1, resonator 1). The fingers of the comb-drive are not visible due to low resolution of optical imaging.

The schematic of the model of a slender beam, subjected to an axial force and carrying an attached lumped mass along its length, is shown in Fig. 2. The governing equation of motion of the beam can be written as follows.

$$\rho A\frac{\partial^2 W}{\partial t^2}+M\delta(x-a)\frac{\partial^2 W(a,t)}{\partial t^2}+J\delta'(x-a)\frac{\partial^3 W(a,t)}{\partial x\partial t^2}+EI\frac{\partial^4 W}{\partial x^4}-P\frac{\partial^2 W}{\partial x^2}=0 \quad (1)$$

where ρ, E, P, A, and I are density, elastic modulus, axial force, cross-sectional area, and area moment of cross-sectional area of the beam, respectively. Parameters M and J are mass and rotary inertia of the lumped mass. In [3], the beam-mass system is treated as two beams connected to each other through the lumped mass. The eigenvalue problem associated with each beam is derived, from which the characteristic equation of the system is obtained. This characteristic equation in dimension-less form is an 8 by 8 matrix with the determinant of zero. In [4], the properties of mode shapes of vibration of Eq. 1 as well as the corresponding orthogonality condition are discussed in detail. For the sake of brevity the results of [2 and 3] will be used in this paper without any further discussion on the modeling of the mechanical system.

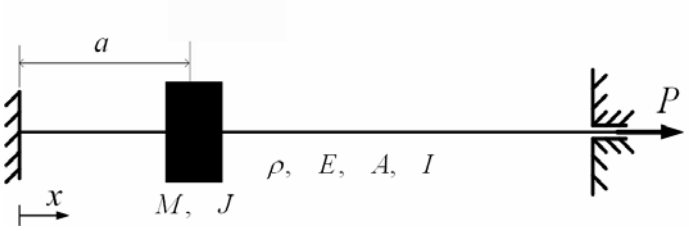

Fig. 2. Model of a resonant beam with attached lumped mass carrying an axial force.

ELECTROSTATIC MODEL

As mentioned earlier, a variety of mechanisms are available for exciting micromachined beam resonators and detecting the resulting vibration, from which electrostatic comb-drive actuator/sensor has the advantage of linearity of the excitation force and sensor output current with respect to the displacement.

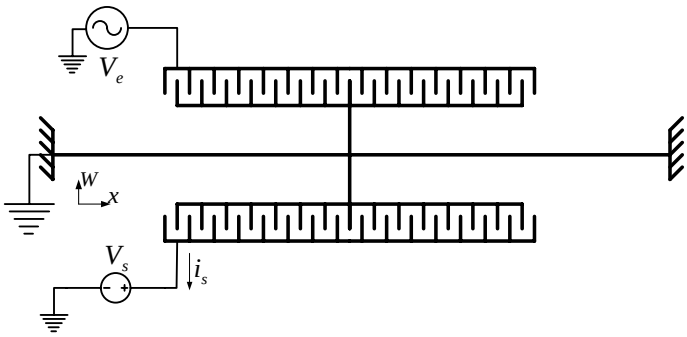

Fig. 3 Electrostatic model of resonant beam with comb-drive actuator/sensor

Fig. 3 shows the configuration of a resonant beam with attached comb-drive actuator/sensor. In this configuration, each comb has N pairs of parallel fingers. The upper comb is used to excite the beam, while the lower comb is utilized to detect the vibration. The capacitance of the excitation comb-drive is [5]

$$C_e=\varepsilon N\frac{h[l_0+W(a,t)]}{g}, \quad (2)$$

where ε is the electric permittivity, h is the thickness of the structural layer, l_0 is the initial overlapping distance, and g is the gap between two parallel fingers. If the excitation voltage of V_e is applied to this comb-drive, the potential energy stored in the comb-drive is

$$U_e = \tfrac{1}{2} C V_e^2 \tag{3}$$

Consequently, the excitation force applied from the electric field can be found by taking the gradient of potential energy [5].

$$F_e = \frac{\partial U_e}{\partial W} = \frac{\varepsilon N h}{2g} V_e^2 \tag{4}$$

Assuming that the excitation voltage consists of both DC and AC component, i.e., $V_e = v_0 + v_a \sin(\omega t)$, one concludes that

$$F_e = \frac{\varepsilon N h}{2g}\left[v_0^2 + \frac{v_a^2}{2} + 2 v_0 v_a \sin(\omega t) - \frac{v_a^2}{2}\cos(2\omega t)\right]. \tag{5}$$

Eq. 5 indicates that an excitation signal with an AC component at the frequency of ω produces an excitation force at the frequency of 2ω. On the other hand, the capacitance of the detecting comb is

$$C_s = \varepsilon N \frac{h[l_0 - W(a,t)]}{g} \tag{5}$$

The output current from the sensing comb-drive is the rate of electric charge stored in the comb. i.e.,

$$i_s = \frac{\partial}{\partial t}(C V_s) \tag{6}$$

where V_s is the voltage at the sensing node and is assumed to be constant. Therefore,

$$i_s = -V_s \frac{\varepsilon N h}{g} \frac{\partial W(a,t)}{\partial t} \tag{7}$$

Thus, the output current of the sensor, i_s, has the same frequency content as the excitation force, F_e, provided that the excitation force is not applied to the node of a vibration mode shape. This means that if the excitation voltage is at the frequency of ω, then the component of the output current at the frequency of 2ω must be measured to verify if the resonance state is achieved [6]. In addition to this technique, phase shift of the signal can be also observed to detect the resonance [5].

EXPERIMENT AND RESULTS

Two micromachined beams are designed and fabricated using the Micragem technology [7]. The choice of fabrication technology has been due to its availability to the authors, and other fabrication technologies could be used. The Micragem is a single crystal silicon on glass fabrication technology with the structural layer thickness of 10 microns. Table 1 lists the geometrical and mechanical properties of the resonators.

Resonator 1 is a resonant beam with the comb-drive actuator/sensor located at the mid-point of the beam, while in resonator 2, the comb-drives are off mid-point. Both resonant beams have same length, however, the theoretical mechanical model suggests that resonator 2 must have higher natural frequencies than resonator 1.

The excitation of the resonant sensors in the air is difficult, because of the damping and squeezed film effect of air molecules on the resonant structure. Thus, a vacuum chamber is designed and utilized to eliminate the effect of air damping. What remains is the structural damping which is very small. The quality factor of resonators working in vacuum is reported in the literature to be more than 1000 [8]. Fig. 4 shows the setup designed for this experiment.

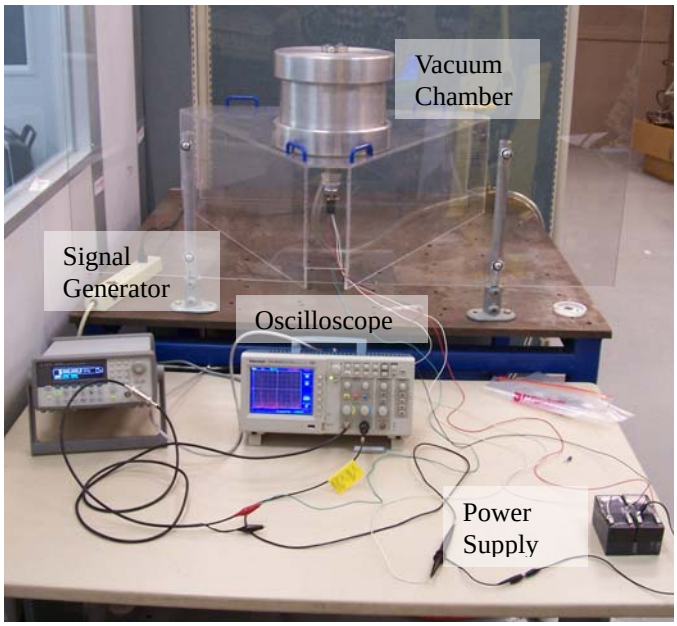

Fig. 4. Experimental setup: vacuum chamber, signal generator, oscilloscope, and batteries for power supply.

An open-loop circuit, similar to the one reported in [6], is used to measure the natural frequencies of these two resonators. An Agilent 33250A is used to provide $V_e = v_a \sin(\omega t)$. The output current of the sensor is immediately amplified and transformed into the voltage fluctuations using a transimpedance amplifier. The amplifying circuit is placed inside the chamber to reduce the parasitic effect of long wiring.

Lead-acid batteries are used as the power supply of the system to minimize the fluctuation of the voltage needed to be applied to the sensing comb-drive.

The FFT mode of a Tektronix TDS2022B oscilloscope is utilized to measure the frequency component of the output current at 2ω. By sweeping the frequency of the excitation voltage, the resonance frequencies are detected. Fig. 5 depicts the voltage of sensor output the frequency domain when the excitation frequency is close to the first resonance of resonator 1. It can be observed that the output voltage has a significant peak at the natural frequency of the resonant beam compared to those at frequencies lower or higher than this frequency.

The experimental first three natural frequencies of each resonator are listed in Table 2. It must be noted that the second resonance of resonator 1 is not detected because the actuator as well as the sensor are located at the mid-span of the beam and are unable to excite and sense the second mode of vibration.

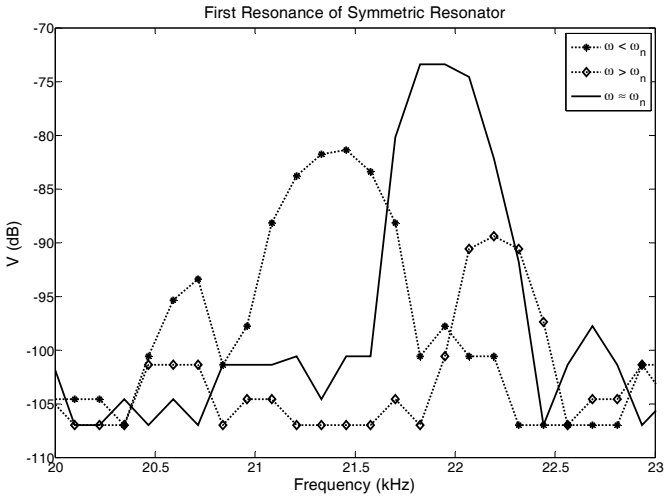

Fig. 5. The open-loop response of the resonator 1 to excitation force at frequencies close to the first resonance frequency.

The parameters in the analytical model are density, modulus of elasticity, axial force of the beam, as well as inertia, and location of the comb-drives. By the time a resonator is designed and fabricated, the location, the radius of gyration and the mass ratio between the combs and the beam are determined and fixed. The density and the modulus of elasticity of the silicon crystal and the axial force of the resonant beam are to be determined using experimental results and the analytical model.

The range of density and modulus of elasticity are known and can be easily found [5]. On the other hand, the axial force may vary from chip to chip or even from location to location and time to time on the same chip. The residual stress due to the bonding between silicon crystal and the glass substrate and the change of temperature are two main sources of the induced axial force. The glue stains under the glass substrate are visible in Fig. 3. This glue that is used to fix the MEMS chip inside its packaging may introduce residual stress to the device. The unevenness of gluing most probably generates uneven stress field in the MEMS structural layer.

Knowing this, density and modulus of elasticity are chosen to be in the ranges reported and the axial force of each resonator is adjusted so that the analytical natural frequencies match with experimental results with minimum deviation. In this paper, the abovementioned parameters are found by trial and error, however, a more reliable and less intuitive approach using optimization techniques, in which the uniqueness of the solution is guarantied, is under study. Table 3 lists the analytical model parameters and their corresponding natural frequencies. The axial stress of each beam is obtained by dividing the axial force by the cross sectional area of each beam from Table 1. The maximum deviation of the analytical natural frequencies from those of experimental results is for the third mode of resonator 2, which is about %6.6, Table 4. This deviation can be justified by the limited bandwidth of the amplifiers and low response amplitude of the resonator at higher modes resulting in the difficulty of output response measurement. In addition, the beam in the analytical model is assumed to be clamped-clamped, however, the boundary conditions of the fabricated resonators are non-ideal, and might have non-zero slopes.

CONCLUSION

The analytical model of the beam-mass system has predicted that the effect of added mass to the resonant beam can be eliminated by proper adjustment of the comb-drive mass, rotary inertia, and location. In addition, the analytical model can predict the effect of the axial force of the beam on the resonance frequencies. In this paper, the results of the experiment on two resonators, fabricated using Micragem technology, have been presented. The first three resonance frequencies have been used to verify the validity of the analytical model as well as determine the axial force of each resonant beam. In addition, the residual stresses of the MEMS chips are calculated using the determined axial forces. Very close agreement between the theory and experiment has been observed.

NOMENCLATURE

A : beam cross-sectional area
a : lumped mass location
C_e : capacitance of excitation comb-drive
C_s : capacitance of sensing comb-drive
E : modulus of elasticity
F_e : excitation force
g : gap between two parallel fingers
h : MEMS structural layer thickness

I : cross-sectional second moment of area
i_s : sensing comb-drive output current
J : lumped mass rotary inertia
L : resonant beam length
l_0 : initial overlapping distance of parallel fingers
M : lumped mass
N : number of parallel finger pairs
P : beam axial force
V_e : excitation voltage
V_s : sensing voltage
v_0 : DC component of excitation voltage
v_a : AC amplitude of excitation voltage
W : beam transverse deflection
ε : electric permittivity
ρ : density of MEMS structural layer
ω : frequency of the excitation voltage

ACKNOWLEDGMENTS

The authors would like to acknowledge the support of the Natural Sciences and Engineering Research Council (NSERC).

REFERENCES

[1] R. Bashir, BioMEMS: state-of-the-art in detection, opportunities and prospects, Advanced Drug Delivery Reviews, 56 (2004) 1565-1586.

[2] P.A. Hassanpour, W.L. Cleghorn, E. Esmailzadeh, J.K. Mills, Exact Solution of the Oscillatory Behavior Under Axial Force of a Beam with a Concentrated Mass Within its Interval, Journal of Vibration and Control. 13 (2007) 1723-1739.

[3] P.A. Hassanpour, W.L. Cleghorn, E. Esmailzadeh and J.K. Mills, Vibration analysis of micro-machined beam-type resonators, Journal of Sound and Vibration, vol. 308 (1-2), 2007, p. 287-301.

[4] P.A. Hassanpour, W.L. Cleghorn, E. Esmailzadeh and J.K. Mills, Generalized orthogonality condition for beams with intermediate lumped masses subjected to axial force. Submitted to the Journal of sound and Vibration, December 2007.

[5] N. Lobontiu & E. Garcia, Mechanics of microelectro-mechanical systems, Kluwer Academic Publishers, 2005.

[6] B. Bahreyni, C. Shafai, A micromachined magnetometer with frequency modulation at the output, Proceedings of the Fourth IEEE Conference on Sensors 2005, p 580-583.

[7] Canadian Microelectronics Corporation, 210A Carruthers Hall, Queen's University, Kingston, Ontario, Canada K7L 3N6. Introduction to Micragem: A Silicon-on-Insulator Based Micromachining Process, 2004.

[8] O. Brand, H. Baltes, Micromachined Resonant Sensors - an Overview; Sensors Update, v 4, n 1, Aug., 1998, p 3-51.

ANNEX A

TABLES

Table 1. Geometrical and mechanical properties of fabricated resonators.

Resonator No.	$L\ (\mu m)$	$a\ (\mu m)$	$A\ (\mu m^2)$	$M\ (kg)$	$J\ (kg.m^2)$
1	1500	750	120	3.89×10^{-10}	3.24×10^{-18}
2	1500	260	120	2.77×10^{-10}	2.30×10^{-18}

Table 2. Experimental results

Resonator No.	F_1 (kHz)	F_2 (kHz)	F_3 (kHz)
1	22.0	N/D	174
2	45.9	101	202

Table 3. Analytical model parameters calibrated based on experimental results

Resonator No.	$\rho\ (kg/m^3)$	$E\ (GPa)$	$P\ (\mu N)$	F_1 (kHz)	F_2 (kHz)	F_3 (kHz)	$\sigma\ (MPa)$
1	2330	145	-420	22.00	138.18	183.10	-3.5
2	2330	145	1200	47.06	96.53	188.72	10

Table 4. Comparison between experimental and analytical model results

	Resonator No. 1			Resonator No. 2		
	F_1	F_2	F_3	F_1	F_2	F_3
Experimental	22.0	N/D	174	45.9	101	202
Analytical	22.00	138.18	183.10	47.06	96.53	188.72
Error (%)	0.0	-	5.2	2.5	4.4	6.6